Research & Reviews: Journal of Material Science

DOI: 10.4172/2321-6212.1000210

e-ISSN: 2321-6212
p-ISSN: 2347-2278
www.rroij.com

Syntheses and Luminescence Enhancement of $Li_{1+x}(Ta_{1-z}Nb_z)_{1-x}Ti_xO_3:RE^{3+}$ (RE=Eu, Er, Tm or Dy) Phosphors

Genki Saitoh[1], Hiromi Nakano[1*], Hiroki Banno[2], and Koichiro Fukuda[2]

[1]Toyohashi University of Technology, Toyohashi, 441-8580, Japan

[2]Nagoya Institute of Technology, Nagoya, 466-8555, Japan

[*]**For Correspondence:** Hiromi Nakano, Toyohashi University of Technology, Toyohashi, 441-8580, Japan, Tel: +81-532-44-6606; E-mail: hiromi@crfc.tut.ac.jp

Received date: Dec 22, 2017, **Accepted date:** Jan 24, 2018, **Published date:** Jan 31, 2018

Research Article

ABSTRACT

We synthesized the phosphors of RE^{3+}-doped $Li_{1+x}(Ta_{1-z}Nb_z)_{1-x}Ti_xO_3$ (LTNT) with various emission colors by solid-state reaction in air using a conventional electric furnace, where RE=Eu, Er, Tm, or Dy. The optimal host composition with each dopant was determined for the highest photoluminescence (PL) intensity; the relevant chemical formulas were $Li_{1.11}Ta_{0.89}Ti_{0.11}O_3$ (x=0.11 and z=0) with Eu^{3+}, $Li_{1.03}(Ta_{0.2}Nb_{0.8})_{0.97}Ti_{0.03}O_3$ (x=0.03 and z=0.8) with Er^{3+}, $Li_{1.08}(Ta_{0.4}Nb_{0.6})_{0.92}Ti_{0.08}O_3$ (x=0.08 and z=0.6) with Tm^{3+}, and $Li_{1.14}(Ta_{0.6}Nb_{0.4})_{0.86}Ti_{0.14}O_3$ (x=0.14 and z=0.4) with Dy^{3+}. The crystal structures of the phosphors were refined by the XRD-Rietveld method to clarify the relationship between the PL properties and crystal structures. In the LTNT host material, the most effective activator was the Eu^{3+} ion, with an internal quantum efficiency of 97%. The efficient PL emission is closely related to the coordination environment of Eu^{3+} in the [Li (Eu) O_{12}] polyhedron of the host LTNT.

Keywords: Oxide phosphors, Photoluminescence, XRD, Rietveld method

INTRODUCTION

In the $Li_2O–Nb_2O_5–TiO_2$ system, the crystals of $Li_{1+x-y}Nb_{1-x-3y}Ti_{x+4y}O_3$ (LNT) with $0.05 \leq x \leq 0.3$ and $0 \leq y \leq 0.182$ form a superstructure known as the M-phase, which was discovered by Villafuerte-Castrejon et al. [1,2]. Several researchers have investigated the origin of this superstructure, and clarified that it is formed by the periodical insertion of an intergrowth layer into a matrix having a basic trigonal basic structure [3-7]. With the crystals of $Li_{1+x-y}Ta_{1-x-3y}Ti_{x+4y}O_3$ (LTT) in the $Li_2O–Ta_2O_5–TiO_2$ system ($0.1 \leq x \leq 0.15$ and $0.05 \leq y \leq 0.175$), there are a few reports mentioning the relationship between the dielectric properties and compositions [8]. However, to the best of the authors' knowledge, there have been no reports on the detailed crystal structures. The compositional ranges of the superstructure formation, together with the periods of the intergrowth layer, were different between the crystals of LNT and LTT. Interestingly, the amount of Ti that was required for the superstructure formation was larger for LTT than for LNT [9].

For the application of LNT as a phosphor host material, rare earth (RE^{3+}=Eu, Er, Tm, or Dy) doped LNT solid solutions have been prepared by heating in air using a conventional electric furnace and/or millimeter-wave furnace [10-12]. The RE^{3+}-doped LTT phosphors were also successfully synthesized, and their photoluminescence (PL) properties were compared to those of LNT:RE^{3+} [13]. Furthermore, we previously reported on a new red-emitting phosphor in the $Li_2O–Nb_2O_5–Ta_2O_5–TiO_2$ system, in which we used the quaternary $Li_{1+x}(Ta_{1-z}Nb_z)_{1-x}Ti_xO_3$ (LTNT, $0 \leq x \leq 0.25$, $0 \leq z \leq 1.0$) solid solution as the host material [14]. The PL intensity of the LTT:Eu^{3+} phosphor, which was found to be dependent on the concentration of Eu^{3+}, showed a high internal quantum efficiency of 84%.

In this work, in order to further improve the PL intensities of the newly developed LTNT:RE^{3+} phosphors, we have clarified the optimal compositions of the host materials for each of the activators RE^{3+}, and the relevant crystal structures. We also discussed the close relationship between the PL properties and crystal structures.

e-ISSN: 2321-6212
p-ISSN: 2347-2278

EXPERIMENTAL PROCEDURE

The starting materials used for the preparation of LTNT were the reagent-grade chemicals of Li_2CO_3, Nb_2O_5, Ta_2O_5, and TiO_2 (>99.9% grade). Each of the rare earth oxides (Eu_2O_3, Sm_2O_3, Er_2O_3, Tm_2O_3, and Dy_2O_3>99.9% grade) was doped in the LTNT solid solution. The powder specimens were well mixed, pressed into pellets, and heated in air at 1423 K for 15 h in a conventional electric furnace.

Phase identification was made based on the X-ray powder diffraction (XRPD) data (CuKα), which were obtained on a RINT 2500 device (Rigaku Co., Ltd., Japan) operated at 40 kV and 200 mA. The phase compositions were determined from the XRPD data (CuKα_1) collected on another diffractometer in the 2θ range of 15.0-100.0° (X'Pert PRO Alpha-1, PAN alytical B.V., Almelo, the Netherlands) operated at 45 kV and 40 mA. The profile intensity data were investigated by the Rietveld method [15] using a computer program RIETAN-FP [16]. The crystal-structure models were visualized with a computer program VESTA [17]. Distortion parameters for the coordination polyhedra were determined using a computer program IVTON [18]. Excitation and emission spectra were obtained using a fluorescence spectrophotometer (F-7000HITACHI, Japan). Quantum efficiency was measured by a spectral radiometer (MCPD-7000, Otsuka Electronics Co., Ltd., Osaka, Japan).

RESULTS AND DISCUSSIONS

Optimal compositions and PL properties of LTNT: RE^{3+} phosphors

In our previous paper, we compared the emission spectra between the two-types of phosphors, RE^{3+}-doped $Li_{1.11}Nb_{0.89}Ti_{0.11}O_3$ (LNT with x=0.11 and y=0) and RE^{3+}-doped $Li_{1.11}Ta_{0.89}Ti_{0.11}O_3$ (LTT with x=0.11 and y=0) as shown in **Figure 1** [13]. The resulting materials showed various emission colors, ranging from red for $Li_{1.11}Ta_{0.89}Ti_{0.11}O_3$:$Eu^{3+}$, yellow for $Li_{1.11}Ta_{0.89}Ti_{0.11}O_3$:$Dy^{3+}$, green for $Li_{1.11}Ta_{0.89}Ti_{0.11}O_3$:$Er^{3+}$, and blue for $Li_{1.11}Ta_{0.89}Ti_{0.11}O_3$:$Tm^{3+}$. With the $Li_{1.11}Ta_{0.89}Ti_{0.11}O_3$ host material, the most appropriate activator for effective emission was the Eu^{3+} ion. On the other hand, when activated with Er^{3+} and/or Tm^{3+}, the emission intensities were lower for $Li_{1.11}Ta_{0.89}Ti_{0.11}O_3$ than for $Li_{1.11}Ta_{0.89}Ti_{0.11}O_3$. Hence, we concluded that the slight differences in the coordination environment of RE^{3+} between the host materials of $Li_{1.11}Ta_{0.89}Ti_{0.11}O_3$ and $Li_{1.11}Ta_{0.89}Ti_{0.11}O_3$ would effectively affect the emission energies of the RE^{3+} ions.

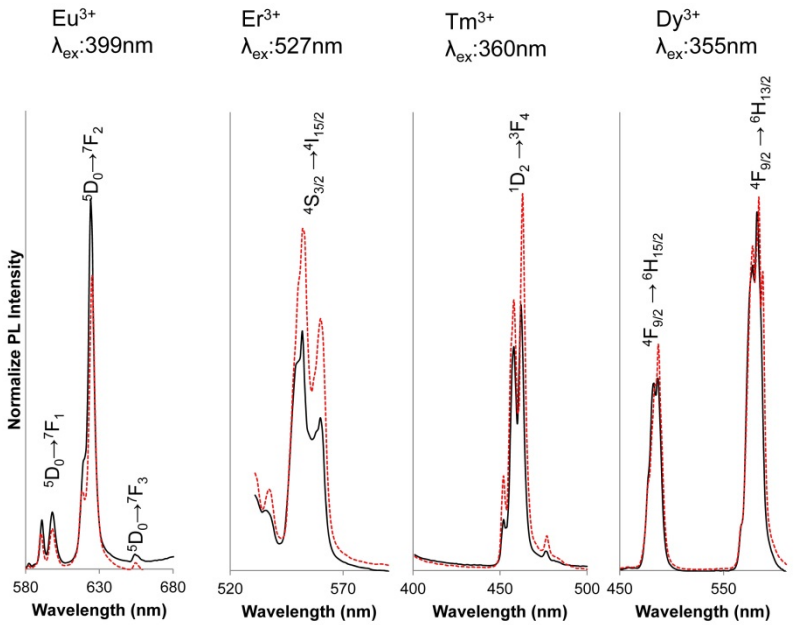

Figure 1. Emission spectra of $Li_{1.11}(Ta/Nb)_{0.89}Ti_{0.11}O_3$:$RE^{3+}$. Dotted line is for LNT:RE^{3+} and solid line is for LTT:RE^{3+} [13].

e-ISSN: 2321-6212
p-ISSN: 2347-2278

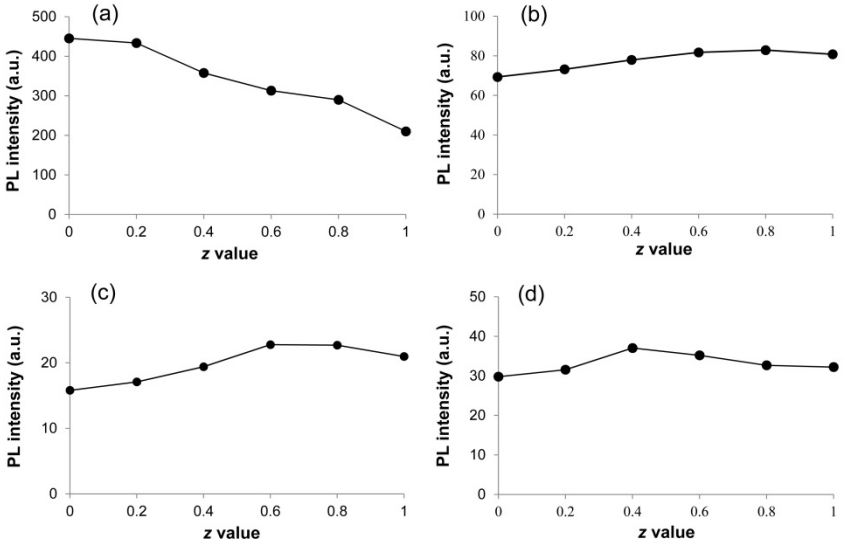

Figure 2. Changes of PL intensities with z values of $L_{1.11}(Ta_{1-z}Nb_z)_{0.89}Ti_{0.11}:RE^{3+}$ (RE_2O_3: 2.5 wt%). Phosphors activated with (a) Eu^{3+}, (b) Er^{3+}, (c) Tm^{3+}, and (d) Dy^{3+}.

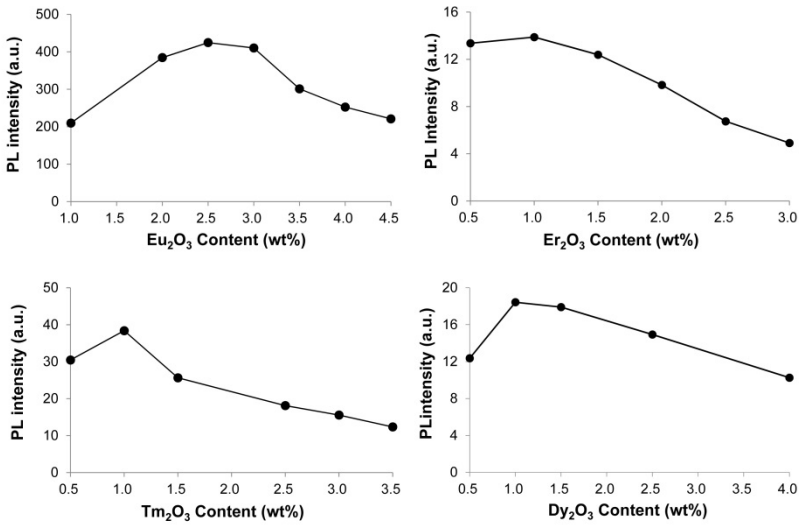

Figure 3. Changes of PL intensities with RE_2O_3 concentrations of $Li_{1.11}Ta_{0.89}Ti_{0.11}O_3:RE^{3+}$. Phosphors activated with (a) Eu^{3+}, (b) Er^{3+}, (c) Tm^{3+}, and (d) Dy^{3+}.

Figure 2 shows the relationship between PL intensity and the z value of $L_{1.11}(Ta_{1-z}Nb_z)_{0.89}Ti_{0.11}:RE^{3+}$ (RE_2O_3: 2.5 wt%). The emission or excitation wavelengths were measured by monitoring them at maximum wavelengths. The PL intensities of the phosphors were measured at 399 nm for Eu^{3+}, at 526 nm for Er^{3+}, at 359 nm for Tm^{3+}, and at 355 nm for Dy^{3+}. We determined the optimal z-values of LTNT (x=0.11) with different RE^{3+} ions; they were z=0 for Eu, z=0.6 for Tm, z=0.8 for Er, and z=0.4 for Dy. We subsequently determined the most suitable quantities of RE^{3+} ions as activators for the host material of $Li_{1.11}Ta_{0.89}Ti_{0.11}O_3$. Among the phosphors doped with Eu_2O_3 up to 4.5 wt%, the highest PL intensity was observed when doped with 2.5 wt% Eu_2O_3 (**Figure 3**). For the other phosphors doped with Er_2O_3 up to 3.0 wt%, those doped with Tm_2O_3 up to 3.5 wt%, and those doped with Dy_2O_3 up to 4.0 wt%, the PL intensities were the highest for 1.0 wt% Er_2O_3, 1.0 wt% Tm_2O_3, and 1.0 wt% Dy_2O_3 (**Figure 3**). Finally, we determined the optimal Ti content in the host materials under the best condition of the z-values and RE_2O_3 contents (**Figure 4**). As a result, the optimal host composition showing the highest PL intensity was eventually determined for each of the dopants; the relevant chemical formulas were $Li_{1.11}Ta_{0.89}Ti_{0.11}O_3$ (x=0.11 and z=0) with Eu^{3+}, $Li_{1.03}(Ta_{0.2}Nb_{0.8})_{0.97}Ti_{0.03}O_3$ (x=0.03 and z=0.8) with Er^{3+}, $Li_{1.08}(Ta_{0.4}Nb_{0.6})_{0.92}Ti_{0.08}O_3$ (x=0.08 and z=0.6) with Tm^{3+}, and $Li_{1.14}(Ta_{0.6}Nb_{0.4})_{0.86}Ti_{0.14}O_3$ (x=0.14 and z=0.4) with Dy^{3+}. In general, the electronic dipole intensities in the lanthanide 4f−4f transitions exhibit extraordinary sensitivity to the ligand environment, hence the optimal host compositions as determined above must be close to those most appropriate in view of the lattice vibrations and environment of RE^{3+} ions.

e-ISSN: 2321-6212
p-ISSN: 2347-2278

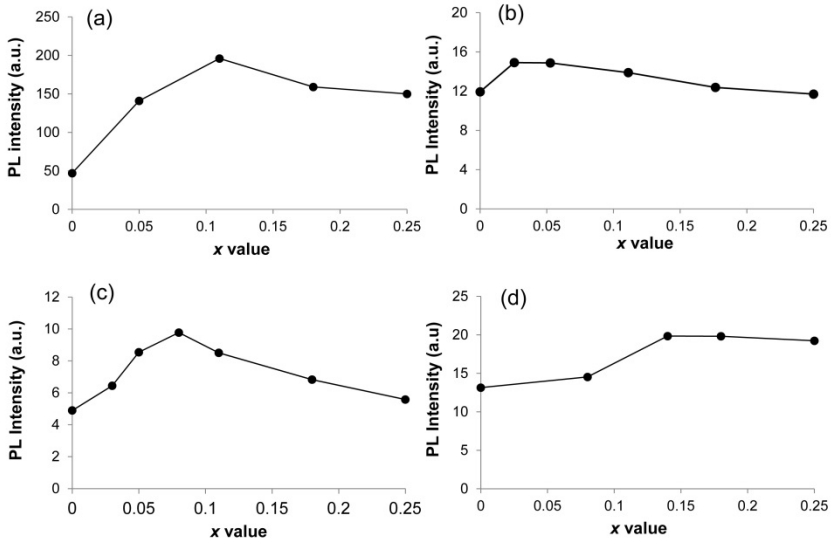

Figure 4. Changes of PL intensities with x-values (concentrations of Ti) of (a) $Li_{1+x}Ta_{1-x}Ti_xO_3:Eu^{3+}$, (b) $Li_{1+x}(Ta_{0.2}Nb_{0.8})_{1-x}Ti_xO_3:Er^{3+}$, (c) $Li_{1+x}(Ta_{0.4}Nb_{0.6})_{1-x}Ti_xO_3:Tm^{3+}$, and (d) $Li_{1+x}(Ta_{0.6}Nb_{0.4})_{1-x}Ti_xO_3:Dy^{3+}$.

In the phosphors emitting various colors, the $Li_{1.11}Ta_{0.89}Ti_{0.11}O_3:Eu^{3+}$ phosphor showed a relatively high internal quantum efficiency of 84% as previously reported [14]. Furthermore, we reported that the Sm^{3+} ion can act as an effective sensitizer for Eu^{3+}-activated phosphors because of the energy transfer process [17]. In the present experimental stage, we synthesized the Eu^{3+} and Sm^{3+} co-doped phosphor, and characterized the PL property. **Figure 5** shows the excitation and emission spectra of $Li_{1.11}Ta_{0.89}Ti_{0.11}O_3:Eu^{3+},Sm^{3+}$, in which the contents of Eu_2O_3 and Sm_2O_3 were, respectively, 0.1 wt% and 2.5 wt%. The sharp emission peaks with relatively strong intensities were observed at a wavelength of around 625 nm ($^5D_0$-$^7F_2$, electric-dipole), when excited by the purple light of 399 nm. The relatively weak emission appeared at wavelengths around 600 nm ($^5D_0$-$^7F_1$, magnetic-dipole transition in the Eu^{3+} ion) and 700 nm ($^5D_0$-$^7F_4$, electric-dipole transition in the Eu^{3+} ion). The inner quantum efficiency of the phosphor achieved 97%, which was very close to the theoretical value.

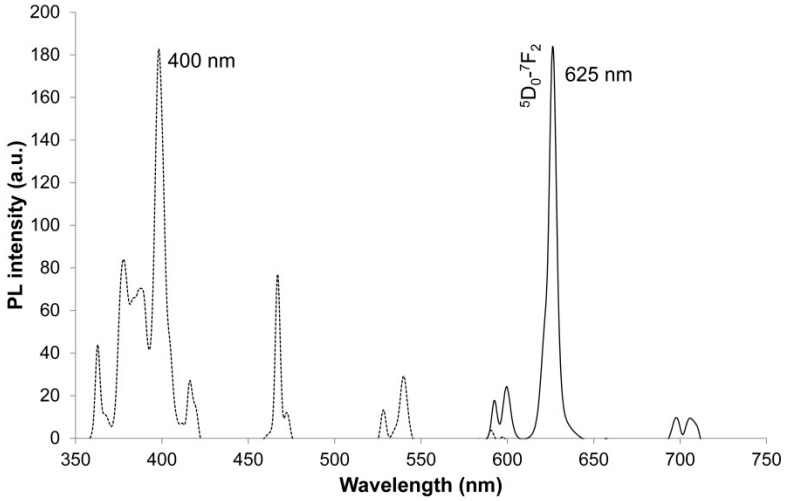

Figure 5. Excitation and emission spectra of $Li_{1.11}Ta_{0.89}Ti_{0.11}O_3:Eu^{3+},Sm^{3+}$.

e-ISSN: 2321-6212
p-ISSN: 2347-2278

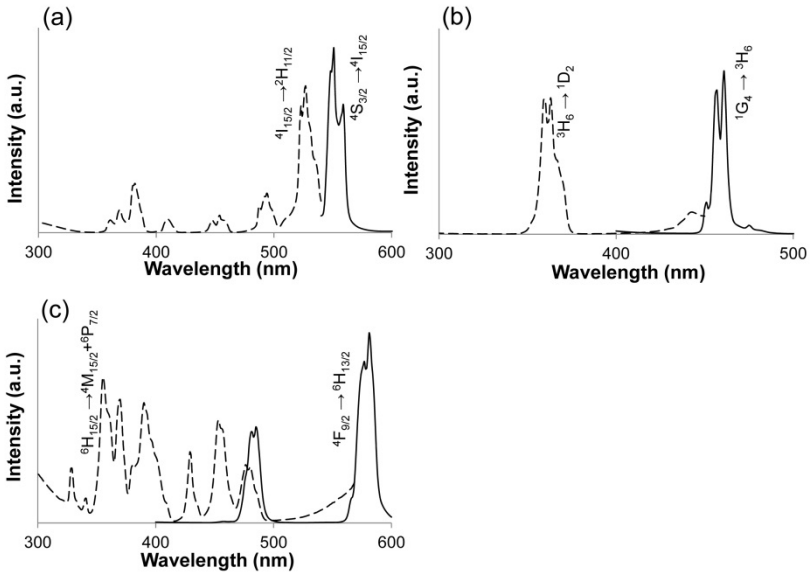

Figure 6. Emission and excitation spectra of (a) $Li_{1.03}(Ta_{0.2}Nb_{0.8})_{0.97}Ti_{0.03}O_3:Er^{3+}$, (b) $Li_{1.08}(Ta_{0.4}Nb_{0.6})_{0.92}Ti_{0.08}O_3:Tm^{3+}$, and (c) $Li_{1.14}(Ta_{0.6}Nb_{0.4})_{0.86}Ti_{0.14}O_3:Dy^{3+}$.

Figure 6 shows the emission and excitation spectra of LTNT phosphors with the most suitable compositions as determined above. **Table 1** summarizes the chromaticity coordinates (x, y) of the emitting light. A green emission peak at 526 nm ($^4S_{3/2}$-$^4I_{15/2}$) was observed for the $Li_{1.03}(Ta_{0.2}Nb_{0.8})_{0.97}Ti_{0.03}O_3:Er^{3+}$ upon excitation at 551 nm ($^4I_{15/2}$-$^2H_{11/2}$). Blue emission was observed at 363 nm ($^1D_2$-$^3F_4$ transition) for the $Li_{1.08}(Ta_{0.4}Nb_{0.6})_{0.92}Ti_{0.08}O_3:Tm^{3+}$ upon excitation at 461 nm ($^3H_6$-$^1D_2$). Yellow emission peaks at around 581 nm ($^4F_{9/2}$-$^6H_{13/2}$) were observed for the $Li_{1.14}(Ta_{0.6}Nb_{0.4})_{0.86}Ti_{0.14}O_3:Dy^{3+}$ upon excitation at 356 nm ($^6H_{15/2}$ -$^4M_{15/2}$). The PL behavior of the RE^{3+}-doped phosphors was not affected by the host material's structure due to the 4f-4f transitions [13,19].

Table 1. Optimal compositions and chromaticity of LTNT phosphors.

Compositions	Chromaticity	
	x	y
$Li_{1.11}Ta_{0.89}Ti_{0.11}O_3:Eu^{3+},Sm^{3+}$	0.675	0.325
$Li_{1.03}(Ta_{0.2}Nb_{0.8})_{0.97}Ti_{0.03}O_3:Er^{3+}$	0.35	0.643
$Li_{1.08}(Ta_{0.4}Nb_{0.6})_{0.92}Ti_{0.08}O_3:Tm^{3+}$	0.146	0.053
$Li_{1.14}(Ta_{0.6}Nb_{0.4})_{0.86}Ti_{0.14}O_3:Dy^{3+}$	0.409	0.385

Morphologies and Crystal Structures of LNTN: RE^{3+} Phosphors

In this chapter, we will discuss the micro-textures and crystal structures of the LTNT:RE^{3+} phosphors. The SEM images in **Figure 7** show that the average grain sizes were about 1.5 μm for $Li_{1.11}Ta_{0.89}Ti_{0.11}O_3:Eu^{3+},Sm^{3+}$, 5.3 μm for $Li_{1.08}(Ta_{0.4}Nb_{0.6})_{0.92}Ti_{0.08}O_3:Tm^{3+}$, 8.0 μm for $Li_{1.03}(Ta_{0.2}Nb_{0.8})_{0.97}Ti_{0.03}O_3:Er^{3+}$, and 4.2 μm for $Li_{1.14}(Ta_{0.6}Nb_{0.4})_{0.86}Ti_{0.14}O_3:Dy^{3+}$. The LNT grain's shape changes from spherical to plate-like when it forms a superstructure [7]. The SEM images indicated that the LTNT:RE^{3+} phosphors had no superstructure because their shapes were not plate-like. The difference in sizes was due to the speed of the grain growth owing to the various doping rare-earth ions and their concentrations. The reflection indices in **Figure 8** were based on the hexagonal unit cells with a ~ 0.5 nm, c ~ 1.4 nm. Parts of the crystal structures of the host materials were determined, and shown in **Figures 9 and 10**. We successfully constructed the structural models, in which all of the RE^{3+} ions occupy the Li site. It should be noted that all of these structures were isomorphous with $LiNbO_3$ (space group R3c), and free from the superstructure peculiar to the M-phase.

e-ISSN: 2321-6212
p-ISSN: 2347-2278

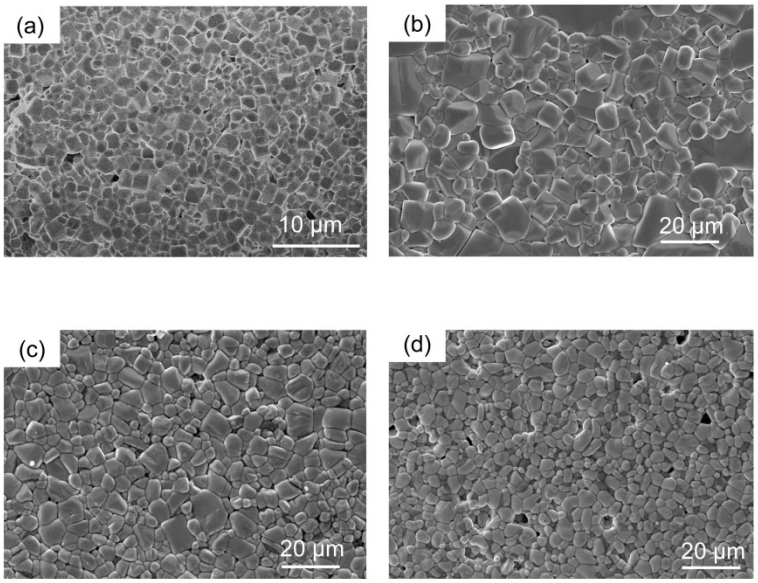

Figure 7. SEM images of (a) $Li_{1.11}Ta_{0.89}Ti_{0.11}O_3:Eu^{3+},Sm^{3+}$,(b) $Li_{1.03}(Ta_{0.2}Nb_{0.8})_{0.97}Ti_{0.03}O_3:Er^{3+}$, (c) $Li_{1.08}(Ta_{0.4}Nb_{0.6})_{0.92}Ti_{0.08}O_3:Tm^{3+}$, and (d) $Li_{1.14}(Ta_{0.6}Nb_{0.4})_{0.86}Ti_{0.14}O_3:Dy^{3+}$.

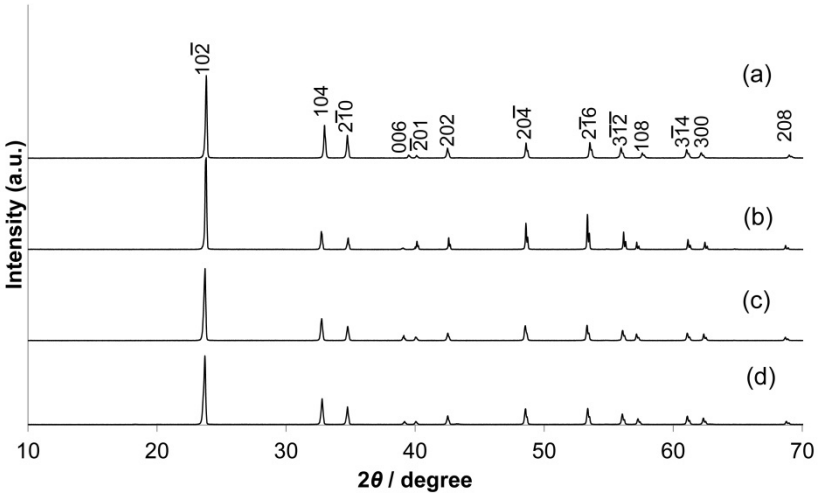

Figure 8. XRD patterns of (a) $Li_{1.11}Ta_{0.89}Ti_{0.11}O_3:Eu^{3+},Sm^{3+}$,(b) $Li_{1.03}(Ta_{0.2}Nb_{0.8})_{0.97}Ti_{0.03}O_3:Er^{3+}$, (c) $Li_{1.08}(Ta_{0.4}Nb_{0.6})_{0.92}Ti_{0.08}O_3:Tm^{3+}$, and (d) $Li_{1.14}(Ta_{0.6}Nb_{0.4})_{0.86}Ti_{0.14}O_3:Dy^{3+}$.

The addition of relatively small amounts of Ti^{4+} effectively increased the PL intensities for $Li_{1+x}Ta_{1-x}Ti_xO_3:Eu^{3+}$ and $Li_{1+x}(Ta_{0.4}Nb_{0.6})_{1-x}Ti_xO_3:Tm^{3+}$ as shown in **Figure 4**. Hence, we refined the crystal structures of $Li_{1+x}Ta_{1-x}Ti_xO_3:Eu^{3+}$ with $0 \leq x \leq 0.25$. **Figure 9** shows parts of the refined structural models of $Li_{0.901}Eu_{0.033}TaO_3$ (x=0), $(Li_{0.977}Eu_{0.023})(Ta_{0.89}Ti_{0.11})O_{2.968}$ (x=0.11), and $(Li_{0.952}Eu_{0.026})(Ta_{0.75}Ti_{0.25})O_{2.901}$ (x=0.25). These chemical compositions were determined as the result of the Rietveld refinement process, and for this reason there are small deviations from those used hitherto. The table included in **Figure 9** describes the polyhedral details of Δ (centroid-to-cation distance; eccentricity), VS (sphere volume), and VP (volume of coordination polyhedron). The distortion-parameter values (VS/VP) of $[(Li, Eu)O_{12}]$ polyhedra were close to each other among the three-types of phosphors with x=0, 0.11, and 0.25, as were the VS/VP-values of $[(Li, Eu)O_{12}]$ polyhedra. However, the $(Li_{0.977}Eu_{0.023})(Ta_{0.89}Ti_{0.11})O_{2.968}$ phosphor (x=0.11) showed a remarkably large Δ-value (= 0.047 nm) in $[(Li, Eu)O_{12}]$ polyhedron as compared with the two other phosphors with x=0 and 0.25. Because the $(Li_{0.977}Eu_{0.023})(Ta_{0.89}Ti_{0.11})O_{2.968}$ phosphor showed the highest PL intensity, the displacement of Eu^{3+} position from the centroid of $[(Li, Eu)O_{12}]$ polyhedra must contribute to the highly enhanced intraconfigurational $^7F_0-^5D_1$ transition.

e-ISSN: 2321-6212
p-ISSN: 2347-2278

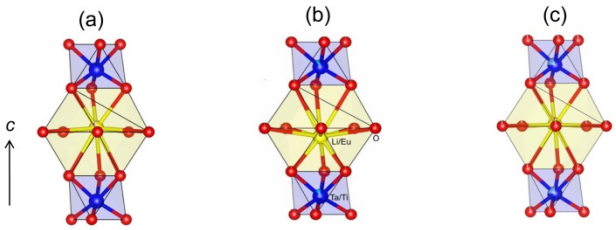

No.	Phosphor's composition	Polyhedron	V_s / nm^3	V_p / nm^3	V_s / V_p	Δ/ nm
(a)	$Li_{0.901}Eu_{0.033}TaO_3$	$[(Li,Eu)O_{12}]$	0.0972	0.0429	2.266	0.017
		$[TaO_6]$	0.0324	0.0103	3.146	0.011
(b)	$(Li_{0.977}Eu_{0.023})(Ta_{0.89}Ti_{0.11})O_{2.968}$	$[(Li,Eu)O_{12}]$	0.0981	0.0429	2.287	0.047
		$[(Ta,Ti)O_6]$	0.0326	0.0104	3.135	0.012
(c)	$(Li_{0.952}Eu_{0.026})(Ta_{0.75}Ti_{0.25})O_{2.901}$	$[(Li,Eu)O_{12}]$	0.0979	0.0431	2.271	0.004
		$[(Ta,Ti)O_6]$	0.0326	0.0103	3.165	0.010

Figure 9. Structural models viewed along [11] and structural data of $Li_{0.901}Eu_{0.033}TaO_3$, $(Li_{0.977}Eu_{0.023})(Ta_{0.89}Ti_{0.11})O_{2.968}$ and $(Li_{0.952}Eu_{0.026})(Ta_{0.75}Ti_{0.25})O_{2.901}$ phosphors.

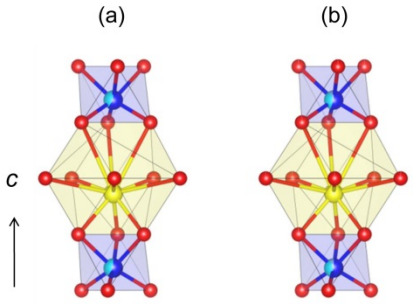

No.	Phosphor's composition	Polyhedron	V_s / nm^3	V_p / nm^3	V_s / V_p	Δ/ nm
(a)	$(Li_{0.991}Tm_{0.007})(Nb_{0.598}Ta_{0.400})O_3$	$[(Li,Tm)O_{12}]$	0.0987	0.0428	2.308	0.065
		$[(Nb,Ta)O_6]$	0.0328	0.0104	3.149	0.017
(b)	$(Li_{0.990}Tm_{0.011})(Nb_{0.558}Ta_{0.361}Ti_{0.081})O_{2.970}$	$[(Li,Tm)O_{12}]$	0.0987	0.0426	2.316	0.064
		$[(Nb,Ta,Ti)O_6]$	0.0327	0.0104	3.147	0.018

Figure 10. Structural models viewed along [11] and structural data of $(Li_{0.991}Tm_{0.007})(Nb_{0.598}Ta_{0.400})O_3$ and $(Li_{0.990}Tm_{0.011})(Ta_{0.361}Nb_{0.558}Ti_{0.081})O_{2.970}$ phosphors.

Figure 10 shows parts of the crystal structures of $(Li_{0.991}Tm_{0.007})(Ta_{0.400}Nb_{0.598})O_3$ and $(Li_{0.990}Tm_{0.011})(Ta_{0.361}Nb_{0.558}Ti_{0.081})O_{2.970}$. These chemical formulas were determined by the Rietveld method, and hence they show slight deviations from the chemical compositions of $Li_{1+x}(Ta_{0.4}Nb_{0.6})_{1-x}Ti_xO_3:Tm^{3+}$ with x=0 and 0.08. The Δ-values as well as the VS/VP-values in $[(Li, Tm)O_{12}]$ polyhedra were almost the same between the two phosphors, although the PL intensity was effectively enhanced for x=0.08 than for x=0 as shown in **Figure 4c**. Thus, the displacement of the Tm^{3+} position from the centroid position of $[(Li, Tm)O_{12}]$ polyhedra would be totally unrelated to the enhancement of PL intensity. Additionally, the displacements of Eu^{3+} and Sm^{3+} positions along the c-axis from the centroid of $[(Eu, Sm)O_{12}]$ polyhedra could be closely related to the enhancement mechanism of the red-light emission through the energy transfer from Sm^{3+} to Eu^{3+} [20,21].

CONCLUSIONS

We synthesized LTNT:RE^{3+} (RE=Eu, Er, Tm, and Dy) phosphors with various emission colors by solid-state reaction in air at 1423 K for 15 h using a conventional electric furnace. The phosphors emitted red light for Eu^{3+}, green light for Er^{3+}, blue light for Tm^{3+}, and yellow light for Dy^{3+}. The optimal host compositions of the phosphors were $Li_{1.11}Ta_{0.89}Ti_{0.11}O_3$ with Eu^{3+}, $Li_{1.03}(Ta_{0.2}Nb_{0.8})_{0.97}Ti_{0.03}O_3$ with Er^{3+}, $Li_{1.08}(Ta_{0.4}Nb_{0.6})_{0.92}Ti_{0.08}O_3$ with Tm^{3+}, and $Li_{1.14}$

$(Ta_{0.6}Nb_{0.4})_{0.86}Ti_{0.14}O_3$ with Dy^{3+}. These compositions would be close to those most appropriate in view of the lattice vibrations and environment of RE^{3+} ions, since the electronic dipole intensities in the lanthanide 4f−4f transitions generally exhibit extraordinary sensitivity to the ligand environment. For the LTNT host phosphor, the most effective activator was the Eu^{3+} ion. The red-emitting phosphor of $Li_{1.11}Ta_{0.89}Ti_{0.11}O_3$: Eu^{3+},Sm^{3+} had a high internal quantum efficiency of 97%. A structural study of the phosphors using the XRD-Rietveld method indicated that the high PL intensity of the Eu^{3+}-activated phosphor was closely related to the environmental symmetry of the Eu^{3+} ion. The displacement of the Eu^{3+} position from the centroid of [(Li, Eu)O_{12}] polyhedra would effectively contribute to the highly enhanced intraconfigurational $^7F_0$−$^5D_1$ transition.

ACKNOWLEDGMENTS

This work was partially supported by a Grant-in-Aid for Scientific Research (c) No. 16K06721 (H. N.) by the Japan Society for the Promotion of Science.

REFERENCES

1. Villafuerte-Castrejon ME, et al. New rutile solid solutions $Ti_{1-4x}Li_xM_{3x}O_2$:M=Nb, Ta, Sb. J Brit Ceram Soc 1984;83:143-145.
2. Villafuerte-Castrejon ME, et al. Compound and solid-solution formation in the system Li_2O-Nb_2O_5-TiO_2. J Solid State Ceram 1987;71:103-108.
3. Smith RI and West AR. Characterization of an incommensurate LiTiNb oxide. Mat Res Bull 1922;27:277-285.
4. Hayashi H, et al. Superstructure in LiTiNb oxides. Forth Ceram Soc 1995;2:391-398.
5. Hayashi H, et al. Preparation of stoichiometric crystalline Li(Nb, Ti)O_3 solid solutions by sol-gel processing with metal alkoxides. Key Eng Mater 1999;161-163:501-504.
6. Farber L, et al. Structural study of $Li_{1+x-y}Nb_{1-x-3}yTi_{x+4}yO_3$ M-Phase solid solutions. J Solid State Chem 2002;166:81-90.
7. Nakano H, et al. Rapid synthesis and structural analysis of Li-Nb-Ti-O solid solutions with superstructure by millimeter-wave heating. J Ceram Soc Jpn 2011;119:808-812.
8. Nakano H, et al. Synthesis and luminescent properties of a new Eu^{3+}-doped Li_{1+x} $(Ta_{1-z}Nb_z)_{1-x}Ti_xO_3$ red phosphor. J Am Ceram Soc 2012;95:2795-2797.
9. Nakano H, et al. Microstructural comparison between Nb- and Ta-systems in $Li_{1+x-y}M_{1-x-3}yTi_{x+4}yO_3$ (M=Nb^{5+}, Ta^{5+}) solid solution with superstructure. J Alloys Comp 2015;618:504-507.
10. Hayashi H and Nakano H. Evaluation and preparation of $Li_{1+x-y}M_{1-x-3}yTi_{x+4}yO_3$ solid solution with superstructure as new phosphor. J Alloys Comp 2010;502:360-364.
11. Hayashi H, et al. Microstructure and luminescence of Eu-doped $Li_{1+x-y}M_{1-x-3}yTi_{x+4}yO_3$ solid solutions with superstructure. J Ceram Soc Jpn 2010;118:226-230.
12. Nakano H, et al. Rapid synthesis of Eu^{3+}-doped LNT (Li-Nb-Ti-O) phosphor by millimeter-wave heating. Opt Mater 2013;35:2045-2048.
13. Nakano H, et al. Synthesis of New RE^{3+} Doped $Li_{1+x}Ta_{1-x}Ti_xO_3$ (RE: Eu, Sm, Er, Tm, and Dy) Phosphors with Various Emission Colors. Materials 2013;6:2768-2776.
14. Nakano H, et al. Synthesis and luminescent properties of a new Eu^{3+}-doped Li_{1+x} $(Ta_{1-z}Nb_z)_{1-x}Ti_xO_3$ red phosphor. J Am Ceram Soc 2012;95:2795-2797.
15. Izumi F and Momma K. Three-dimensional visualization in powder diffraction. Solid State Phenom 2007;130:15-20.
16. Brindley GW. The effect of grain or particle Size on x-ray reflections from mixed powders and alloys, considered in relation to the quantitative determination of crystalline substances by x-ray methods. Philos Mag 1945;36:347-369.
17. Momma K and Izumi F. VESTA 3 for three-dimensional visualization of crystal, volumetric andmorphology data. J Appl Crystallogr 2011;44:1272-1276.
18. Balic-Zunic T and Vickovic I. IVTON – a program for the calculation of geometrical aspects of crystal structures and some crystal chemical applications. J Appl Crystallogr 1996;29:305-306.].
19. Nakano H, et al. Synthesis and luminescence enhancement of Eu^{3+}, Sm^{3+} co-doped $Li_{1.11}Ta_{0.89}Ti_{0.11}O_3$ phosphor. Mater Res Bull 2014;60:766-770.

e-ISSN: 2321-6212
p-ISSN: 2347-2278

20. Yan B and Su X-Q. $LuVO_4:RE^{3+}$ (RE=Sm, Eu, Dy, Er) phosphors by in-situ chemical precipitation construction of hybrid precursors. Opt Mater 2007;29:547-551.

21. Lee G-H, et al. Effect of local environment and Sm^{3+}-codoping on the luminescence properties in the Eu^{3+}-doped potassium tungstate phosphor for white LEDS. J Lumin 2008;128:1922-1926.